RSC Advances

PAPER

View Article Online
View Journal | View Issue

Cite this: *RSC Adv.*, 2024, **14**, 7206

Mechanism of SO_2/H_2O enhanced rare earth tailings catalysts in NH_3-SCR at medium and high temperature

Kunling Jiao,[ab] Jiaming Liu,[a] Xiaoyun Jiao,[a] Siying Wang,[a] Jingran Zhang[a] and Wenfei Wu *[ab]

Received 23rd December 2023
Accepted 12th January 2024

DOI: 10.1039/d3ra08782d

rsc.li/rsc-advances

Rare earth tailings (RET) NH_3-SCR catalysts were prepared by mechanical and microwave activation of a large amount of rare earth tailings after beneficiation of Bayan Ebo rare earth ore. The effects of SO_2/H_2O on the denitrification performance of the RET catalysts were evaluated by conducting denitrification activity tests, SO_2/H_2O tolerance tests and *in situ* DRIFTs mechanistic analysis. The results showed that the denitrification activity was significantly increased in the presence of SO_2/H_2O. And *in situ* DRIFTs analysis showed that in the presence of SO_2/H_2O, SO_2 could be adsorbed as SO_3^{2-} groups by the hydroxyl groups on the catalyst surface and react with SO_4^{2-} to form $S_2O_7^{2-}$ species. And in the presence of NH_3, $S_2O_7^{2-}$ would decompose into unstable SO_4^{2-} species and SO_3^{2-} and continue to react cyclically to form $S_2O_7^{2-}$ species, providing the RET catalyst provides more acid sites, facilitating the SCR reaction.

1 Introduction

NO_x is considered to be one of the serious air pollutants and its main source is industrial combustion emissions from fossil fuels in thermal power plants. NH_3-SCR technology is an effective method for NO_x removal.[1–3] V_2O_5–$WO_3(MoO_3)/TiO_2$ has been used industrially for many years,[4,5] but its applicable denitrification temperature range is narrow. To broaden or reduce the applicable temperature range, researchers have carried out work on the preparation of NH_3-SCR catalysts using transition metal elements,[6–13] which mainly focused on Mn-based, Fe-based and rare earth-based catalysts. It was found that Mn-based catalysts have a good De-NO_X activity in the low temperature band but poor SO_2/H_2O tolerance.[6–8] Fe-based catalysts have some activity (lower than Mn-based catalysts) in the medium to high temperature band (150–450 °C) and have better SO_2 tolerance.[9–13] Single metal oxide catalysts usually have certain defects, so they are usually loaded with other elements to form composite metal oxides for the preparation of the NH_3-SCR catalysts to compensate for each other's defects.

Bayan Ebo has a large amount of rare earth tailings after beneficiation, which contains a rich variety of NH_3-SCR active elements (Fe, Ce, Mn),[14] of which rare earth elements are excellent NH_3-SCR catalyst active components.[15] In addition, there are congenial relationships such as adjacency, leaching and encapsulation of various active minerals in rare earth tailings, and the interactions that exist between these congenial minerals can also facilitate the SCR reaction process,[16,17] so rare earth tailings are naturally excellent materials that can be used to prepare NH_3-SCR catalysts.

SO_2/H_2O poisoning phenomenon seriously affects the activity of SCR catalysts. Due to the increase of HSO_4^- and SO_4^{2-} on the catalyst surface, it often leads to accumulation of ammonium sulfate on the catalyst surface and irreversible sulfation of the active components of the catalyst leading to decreased activity. So improving the SO_2/H_2O tolerance of catalysts is directly related to the practical application of catalysts and is an unavoidable indicator in the evaluation of NH_3-SCR catalysts. Composite oxide catalysts doped with rare earth elements exhibit better SO_2/H_2O tolerance and denitrification efficiency compared to Fe-based and Mn-based denitrification catalysts.[18–21] In contrast, rare earth tailings with multiple active components (Fe, Ce, Mn) are natural composite oxides, and rare earth tailings catalysts have better SO_2/H_2O tolerance performance than most composite oxide catalysts.

Therefore, it is necessary to investigate the SO_2/H_2O tolerance characteristics of the Bayan Ebo rare earth tailings catalysts (RET) in the NH_3-SCR denitrification process and to investigate the SO_2/H_2O tolerance mechanism in the denitrification process. This paper explores the process and tolerance mechanism of SO_2/H_2O on the denitrification performance of the RET catalysts and expands the research field of NH_3-SCR denitrification with rare earth tailings catalysts from Bayan Ebo.

[a]*School of Energy and Environment, Inner Mongolia University of Science and Technology, Baotou, Inner Mongolia Autonomous Region, 014010, China. E-mail: jklgroup1984@163.com*

[b]*Key Laboratory of Efficient and Clean Combustion, Inner Mongolia, China*

Table 1 Rare earth tailings catalyst (RET) XRF results

Element	Fe	Ca	Si	Mg	Ce	Al	Mn	Other
Percentage (%)	17.394	17.798	8.804	3.104	1.783	1.485	0.926	48.706

2 Materials and methods

2.1 Catalysts preparation

The rare earth tailings catalyst was prepared by ball mills. And the rare earth tailings come from Bayan Ebo (Baotou, China). The beneficiated rare earth tailings material was fixed in a canister on a planetary ball mill and ball milled at 300 rpm for 2 h. The obtained material was passed through a 200 mesh sieve and microwave roasted at 1100 w, 250 °C for 20 min to obtain the catalyst powder. The elemental content of the catalyst was quantified by XRF. As shown in Table 1, the results of the XRF analysis, in which Fe, Ca, Si, Mg, Ce and Al were the major elements with a total content of 50.4%, and the remaining 49.6% are Mn and other trace elements, and the content of each trace element is <1%. The Bayan Ebo rare earth tailings catalyst is indicated as RET.

2.2 Catalytic performance experiment

The NH_3-SCR performance experiments with the RET catalysts were carried out in a SCR denitrification evaluation unit, as shown in Fig. 1. The denitrification evaluation unit is consisted of gas distribution system (1–4), reaction system (5–8) and analysis system (9–11), and is equipped with a tail gas treatment unit (12). The sample is fixed in a 9 mm inner diameter quartz fixed bed reaction tube. The reaction gas mixture consists of NO (500 ppm), NH_3 (500 ppm), H_2O (6 vol% when in use), SO_2 (500 ppm when in use), O_2 (6 vol%) and N_2 are controlled by the gas distribution system at a flow rate (100 mL min^{-1}), and the GHSV are set to 30 000 h^{-1}. The gas mixture were measured by on-line multi-component flue gas analyzer (HP-OMGA, China), the measurement accuracy is ≤± 2% FS, and the NO_X conversion is obtained from the formula (1):

$$NO_x\ \text{conversion}(\%) = \frac{[NO_x]_{in} - [NO_x]_{out}}{[NO_x]_{in}} \times 100\% (x = 1, 2) \quad (1)$$

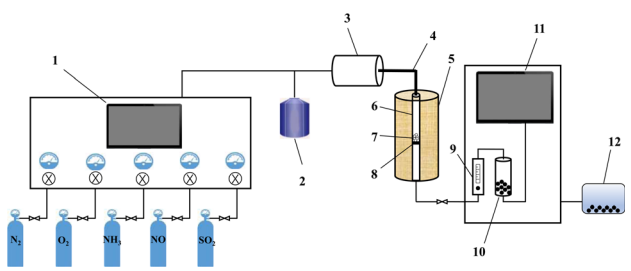

Fig. 1 Schematic diagram of the NH_3-SCR evaluation unit ((1) gas flow control system; (2) heating water tank; (3) gas distribution tank; (4) heating pipes; (5) heating furnace; (6) quartz tubes; (7) RET catalyst; (8) quartz wool; (9) rotameter; (10) condensation drying device; (11) flue gas online detection device; (12) tail gas treatment device).

2.3 Catalysts characterization

The RET catalysts were characterization by the X-ray diffraction (XRD), temperature programmed reduction by H_2 and NH_3 (H_2-TPR and NH_3-TPD), and *in situ* Diffuse Reflectance Infrared Fourier Transform Spectroscopy (DRIFTS).

3 Results and discussion

The RET catalysts after denitrification under different operating conditions were characterised as sample 0, 1, 2 and 3. The total flow rate for all operating condition cases is 100 mL min^{-1}, as shown in Table 2.

3.1 Structural changes of catalysts

As shown in Fig. 2, the diffraction peaks of fluorite (CaF_2), quartz (SiO_2), aluminium trioxide (Al_2O_3), iron dolomite {$Ca(MgFe)[(CO_3)_2]$}, hematite (Fe_2O_3) and cerium fluoride ($CeCO_3F$) were mainly detected on the surface of sample 0, where the $Ca(MgFe)[(CO_3)_2]$, Fe_2O_3 and $CeCO_3F$ diffraction peaks are overlap, it is due to the natural action of these reactive minerals to form a solid solution structure.[18,19] In comparison to sample 0, no significant crystalline phase changes were observed for sample 1 when the catalyst was reacted under H_2O conditions for 24 hours. However, when the catalyst was reacted

Table 2 Working conditions for the preparation of the four RET catalysts

Catalysts	NH_3/ppm	NO/ppm	O_2/%	H_2O/%	SO_2/ppm
Sample 0	500	500	6	—	—
Sample 1	500	500	6	6	—
Sample 2	500	500	6	—	500
Sample 3	500	500	6	6	500

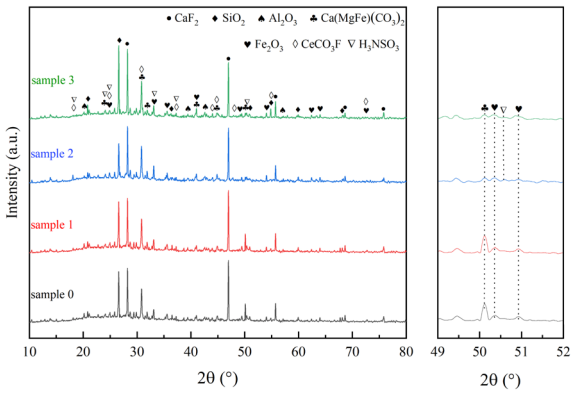

Fig. 2 Rare earth tailings catalyst (RET) XRD results.

under SO_2 or SO_2 and H_2O conditions for 24 hours, a decrease in the intensity of the $Ca(MgFe)[(CO_3)_2]$ and Fe_2O_3 diffraction peak intensities was found for samples 2 and 3, but no characteristic metal sulphate peaks were detected, indicating that the SO_2 sulphide phase was present in an amorphous form and could not be observed by XRD. However, in the presence of SO_2 or SO_2/H_2O, new diffraction peaks were observed for samples 2, 3 at 18.43°, 24.17°, 24.84°, 33.14°, 37.02° and 50.68°, which can be attributed to sulphonate (NH_3SO_3) (PDF#08-0483). And these diffraction peaks overlap with or are similar to the active mineral diffraction peaks of $Ca(MgFe)[(CO_3)_2]$, Fe_2O_3 and $CeCO_3F$. It can be inferred that the newly formed crystalline phase NH_3SO_3 is produced because the acid groups formed on the catalyst surface after SO_2/H_2O is involved in the denitrification process and during the drop to low temperature interact with the NH_3 adsorbed species and a reduction reaction occurs to reduce the active metal centres in the active minerals to their original state.[22–24]

3.2 Catalyst performance change

To examine the effect of SO_2/H_2O on the NH_3 adsorption of the RET catalyst as shown in Fig. 3. The peak temperatures of the desorption peaks of sample 0 were 147 °C (weak acid centers), 356 °C (medium centers) and 480 °C (strong centers).[25] The NH_3 adsorption capacity of samples 1, 2 and 3 was significantly higher than sample 0, while the NH_3 adsorption capacity of samples 2 and 3 was slightly higher than sample 1. Sample 0 showed a desorption peak at 147 °C corresponding to the weak acid site, a desorption peak at 356 °C corresponding to at the medium to strong acidic site, and a desorption peak at 480 °C corresponding to the strong acidic site. At 480 °C corresponds to the desorption peak from the strongly acidic site. Samples 1, 2 and 3 also showed three peaks in the low and medium-high temperature sections, each acidic site being shifted back and enhanced compared to sample 0, indicating that the presence of a suitable amount of SO_2/H_2O can strengthen the acidic sites on the RET catalyst. The peak at 150 °C for sample 3, which was influenced by the combined presence of SO_2/H_2O, was attributed to the weakly acidic sites, with a significantly greater ability to adsorb NH_3 on the weakly acidic sites relative to the RET

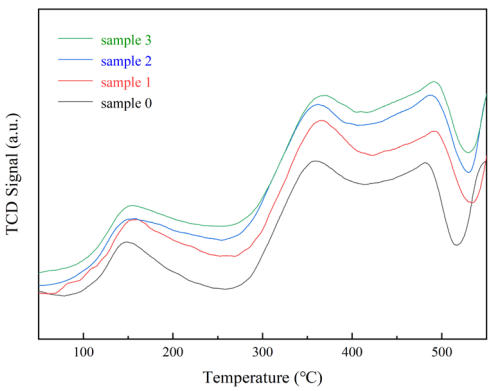

Fig. 3 Rare earth tailings catalyst (RET) NH_3-TPD results.

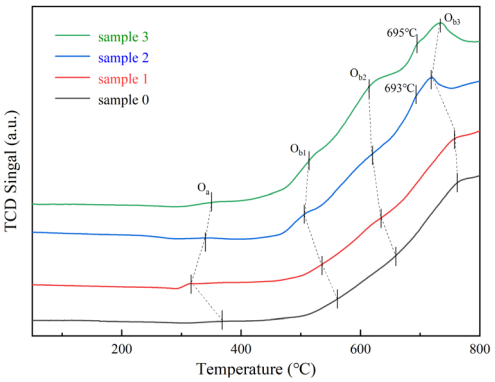

Fig. 4 Rare earth tailings catalyst (RET) H_2-TPR results.

catalysts influenced by the presence of SO_2 or H_2O alone with larger desorption peaks at 365 °C and 489 °C attributed to the moderately strong and strong acidic sites. Significantly larger peak areas in the mid to high temperature fractions compared to samples 1 and 2, which were affected by SO_2/H_2O alone. It means that co-modification of SO_2 and H_2O can also substantially enhance the ability of medium to strong acidic sites to adsorb NH_3. Overall, the RET catalyst with the influence of SO_2/H_2O both increased the acidic sites and improved NH_3 adsorption capacity. Combined with XRD analysis, it was found that the increase in acidic sites after the catalyst was affected by SO_2/H_2O can be attributed to the formation of NH_3SO_3, which is readily decomposed by heat, thus providing more acidic sites.

H_2-TPR tests were using to investigate the effect of the SO_2/H_2O on the redox ability of the RET catalyst. In Fig. 4, the O_a peak located below 400 °C is the reduction peak of oxygen species adsorbed on the catalyst surface. The O_{b1} peak located between 400 and 600 °C is the peak of H_2 consumption (Fe_2O_3 to Fe_3O_4 and the reduction of the CeO_2).[26,27] The O_{b2} peak between 600 and 700 °C is the peak of H_2 consumption (Fe_3O_4 to FeO).[26] The O_{b3} peak above 700 °C is the peak of H_2 consumption (FeO to Fe).[26] The reduction peaks of the RET catalysts with SO_2 or SO_2/H_2O are shifted towards a lower temperature region and the peak area is slightly increased compared to the RET catalysts without the influence of SO_2 or H_2O. This means that SO_2 and H_2O can influence the RET catalysts to induce a beneficial change in redox capacity towards a more beneficial catalytic reduction reaction occurring, with new shoulder peaks are due to the reduction of the CeO_2 at 693 °C and 695 °C,[27] and the introduction of SO_2/H_2O leads to a more pronounced shoulder peak shape at 695 °C. Which combined with XRD analysis, is presumed to be due to the influence of SO_2, which induces the reduction of RET catalysts with the natural co-occurrence of active minerals associated properties of the RET catalyst resulted from the joint participation of multiple substances in the redox reaction.[28] From the H_2-TPR results, electron transfer paths can be derived ($Fe^{3+} \leftrightarrow Fe^{2+}$ and $Ce^{4+} \leftrightarrow Ce^{3+}$).

The surface of the rare earth tailings catalyst (Fig. 5a) showed an uneven and pitted morphology, and the surface of the rare earth tailings catalyst (Fig. 5b) did not change much after the

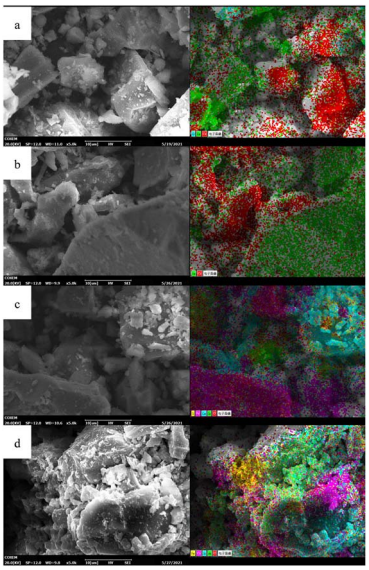

Fig. 5 SEM and EDS surface sweeps before and after the effect of SO_2/H_2O on RET catalysts ((a) fresh RET catalyst; (b) after H_2O; (c) after SO_2; (d) after SO_2/H_2O).

H_2O tolerance test. After being affected by SO_2 alone and SO_2/H_2O tolerance, the catalysts (Fig. 5c and d) showed some mobility, which was in the form of stacked lamellar fragmentation with a few fine particles attached to the surface, after being affected by SO_2/H_2O tolerance, there was a large volume of lamellar particles stacked on the surface of the catalysts, and after the catalysts were affected by the simultaneous presence of SO_2 and H_2O, the lamellar particles were attached to the surface of the catalysts.

3.3 *In situ* DRIFTs analysis

3.3.1 Effect of H_2O on the adsorption of SO_2 on the catalyst surface. The adsorption of SO_2 in the presence of H_2O at 350 °C was investigated by *in situ* DRIFTS, as shown in Fig. 6.

As shown in Fig. 6, the RET catalyst was exposed to SO_2/O_2 for 60 min and treated in a pure N_2 gas stream (100 mL min^{-1}) at 350 °C for a further 30 min. 5 min after the addition of H_2O, an absorption peak of molecular water (1647 cm^{-1}) appeared, with little change in peak intensity with increasing time, meaning that the H_2O tolerance of the RET catalyst was good. The absorption peak of sulfite (1434 cm^{-1}) disappeared with increasing time and the absorption peak of pyrosulfate (1396 cm^{-1}) gradually became stronger. The absorption peaks of bridged tri-dentate sulphate (1326 cm^{-1}), double-dentate sulphate (1076 cm^{-1}), bridged double-dentate sulphate (1197 cm^{-1}) and single-dentate sulphate (1261 cm^{-1}) showed little change.[31,32,35,36] The crystalline water variable angle vibrational peak shifted from 1535 to 1581 cm^{-1}, it is due to the chemisorption of gaseous SO_2 onto the catalyst surface *via* hydroxyl groups.[37] The increase in persulphate is due to the presence of H_2O, which causes the formation of hydroxyl groups on the RET catalyst surface, and adsorb more SO_2 to form SO_3^{2-}, which in turn reacts with the catalyst surface sulphate species to form $S_2O_7^{2-}$, so H_2O promotes the formation of $S_2O_7^{2-}$ species on the RET catalyst surface.

3.3.2 Effect of SO_2/H_2O on surface acidity. Fig. 7 shows that NH_3 was first adsorbed without SO_2 for 60 min at 350 °C and then treated in a pure N_2 gas stream (100 mL min^{-1}) for a further 30 min.

Fig. 7 shows the absorption peaks of NH_4^+ adsorption at the Brønsted acid site (1392, 1427, 1461, 1500 cm^{-1}), NH_3 adsorption at the Lewis acid site (1025, 1157, 1228, 1620 cm^{-1}) and it causes NH_3 form –NH_2 (1332 cm^{-1}).[29,30] After continuing the ammonia stream and 5 min of SO_2, H_2O and O_2, the absorption peaks of NH_4^+ adsorption (1392, 1461 cm^{-1}) and NH_3 adsorption at the Lewis acid site (1157, 1228, 1620 cm^{-1}) disappeared. The intermediate product –NH_2 (1529 cm^{-1})[29,30] and NH_3 adsorption (1600 cm^{-1})[29,30] with increasing peak intensity with time, meaning that the presence of SO_2/H_2O promoted NH_3 adsorption. Bidentate sulfate (1068 cm^{-1}), bridged bidentate sulfate (1191 cm^{-1}), and monodentate sulfate (1265 cm^{-1}) absorption peaks were also present after 40 min.[31,35,36] The intensity of the bidentate and bridged bidentate sulfate absorption peaks frequently changes but no pyrosulfate species were found at 1391 cm^{-1}. In combination with XRD analysis, was attributed to the formation of NH_3SO_3 from NH_3 adsorbed species bound to the catalyst surface. After 40 min of addition of SO_2, H_2O and O_2, the intermediate product –NH_2 (1300,

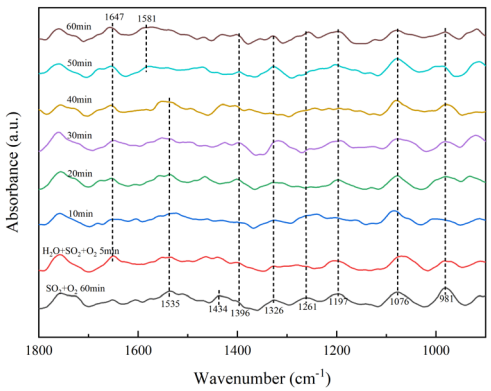

Fig. 6 Effect of H_2O on the adsorption of SO_2 by the RET catalyst.

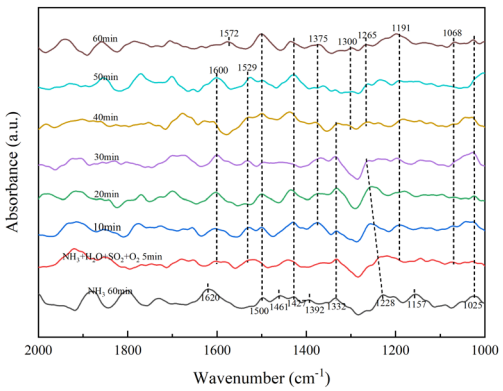

Fig. 7 Effect of SO_2/H_2O on catalyst NH_3 adsorption.

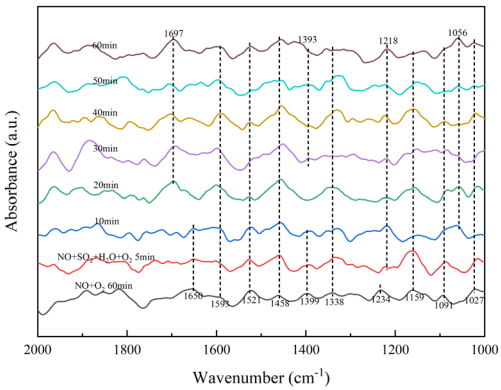

Fig. 8 Effect of SO_2/H_2O on NO adsorption by RET catalysts.

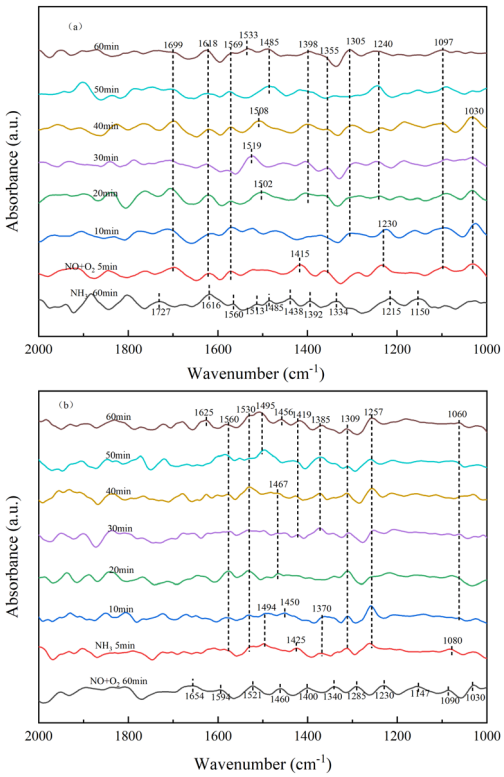

Fig. 9 RET Catalytic transient reaction in the presence of SO_2/H_2O ((a) NH_3/NO; (b) NO/NH_3).

1572 cm^{-1}) appeared, resulting from the creation of a new Lewis acid site, which is consistent with NH_3-TPD results. SO_2/H_2O caused the formation of an unstable sulphate species, which adsorbed on the active metal sites are strongly acidic, so this unstable sulphate species provides more acidic sites for the NH_3-SCR process and is less likely to form ammonium sulphate species with NH_3. The combination of NH_3 with catalyst surface species to form NH_3SO_3 resulted in the disappearance of persulphate species from the RET catalyst surface, indicating that the presence of NH_3 promoted the decomposition of $S_2O_7^{2-}$.

3.3.3 Effect of SO_2 on the adsorbed NO species. As in step with Fig. 8, the *in situ* DRIFTS spectra showed the effect of SO_2/H_2O on NO adsorption on the RET catalyst at 350 °C.

In Fig. 8, the addition of NO and O_2 gas streams followed by a pure N_2 gas stream shows monodentate nitrite (1027, 1091, 1159 cm^{-1}), bridged nitrite (1234 cm^{-1}), intermediate product-NO_2 (1338, 1399, 1458 cm^{-1}), intermediate product-NO_3 (1521 cm^{-1}) and adsorbed NO_2 (1593, 1650 cm^{-1}).[33,34] After simultaneous introduction of NO, O_2, H_2O and SO_2 for 5 min, the absorption peak of bridged nitrite shifted from 1234 to 1218 cm^{-1} with little change in peak intensity with increasing time, with bridged nitrite still occupying the active site. After 10 min of addition of H_2O and SO_2, the absorption peaks of –NO_2 (1399 cm^{-1}) and adsorbed NO_2 (1650 cm^{-1}) disappeared and absorption peaks of bidentate sulfate (1056 cm^{-1}), pyrosulfate (1393 cm^{-1}) and NO_2 (1697 cm^{-1}) generated by the reaction of adsorbed NO on the surface appeared.[33,34,38] In the presence of SO_2/H_2O, the absorption peak of $S_2O_7^{2-}$ species gradually increased with time and the –NO_2 disappeared, due to the competition between SO_2 and NO adsorption on this active site to produce $S_2O_7^{2-}$ species. It occupies part of the NO adsorption site, and the increase in surface active oxygen species due to SO_2 acidification of the RET catalyst, converting more NO to NO_2 and hence the absorption peak of NO_2.

3.3.4 Transient reactions of NH_3 and NO on the catalyst surface. As shown in Fig. 9a, the *in situ* DRIFTs spectra of the reaction of NO with pre-adsorbed NH_3 species on the RET catalyst surface under the influence of SO_2/H_2O and Fig. 9b shows the *in situ* DRIFTs spectra of the reaction of NH_3 with pre-adsorbed NO species on the RET catalyst surface under the influence of SO_2/H_2O.

As shown in Fig. 9a, the RET catalysts were firstly exposed to NH_3 gas flow for 60 min in the addition of SO_2/H_2O, and then purged with N_2 at 350 °C for 20 min.

Fig. 9a shows the absorption peaks of NH_4^+ adsorption (1392, 1438, 1485, 1513, 1727 cm^{-1}), NH_3 adsorption (1150, 1215, 1616 cm^{-1}) and –NH_2 (1334, 1560 cm^{-1}).[29,30] After 5 min of the addition of NO and O_2, the NH_3 adsorbed species disappeared and peaks appeared for monodentate nitrite (1030, 1097 cm^{-1}), bridged nitrite (1230 cm^{-1}), intermediate product –NO_2 (1355, 1415, 1618 cm^{-1}), bidentate nitrate (1569 cm^{-1}) and NO_2 (1699 cm^{-1}).[33,34] The peak of –NO_2 (1415 cm^{-1}) disappeared rapidly with increasing time. The peak pattern of bridged nitrite shifted from 1230 to 1240 cm^{-1} with little change in peak intensity. Monodentate nitrite (1097 cm^{-1}) and bidentate nitrate (1569 cm^{-1}) showed little change. Absorption peaks for intermediate product-NO_2 (1305, 1398 cm^{-1}) and intermediate product-NO_3 (1502 cm^{-1}) appeared after 20 min of the addition of NO/O_2. Absorption peaks of –NO_3 at 1519, 1508, 1485 and 1533 cm^{-1} appeared, with significant changes in peak pattern with increasing time. The absorption peaks of –NO_2 did not change much after 20 min of NO/O_2 addition, and the peak intensity increased. This is due to the fact that when NO/O_2 were first added, the NH_3 adsorbed species mainly combined with –NO_2 to form the intermediate product, and after 20 min as NO was oxidized to more NO_2, the –NO_3 group was generated to participate in the reaction. The results show that –NO_2 is easier to combine with NH_4^+ than –NO_3 to form the intermediate product NH_4NO_2. And when NH_3 is present, the NO species

mainly form the $-NO_2$ group directly to participate in the reaction, without oxidation between the catalyst and NO_2 to form the $-NO_3$ group, shortening the reaction process in favor of the NH_3-SCR reaction.

In Fig. 9b, the samples were first exposed to NO and O_2 for 60 min in the presence of SO_2/H_2O, and then treated in a pure N_2 gas stream (100 mL min^{-1}) at 350 °C for a further 30 min. The appearance of monodentate nitrite (1030, 1090, 1147 cm^{-1}) was observed in Fig. 9b, with bridging nitrite (1230 cm^{-1}), $-NO_2$ (1285, 1340, 1400, 1460 cm^{-1}), $-NO_3$ (1521 cm^{-1}) and adsorbed NO_2 (1594, 1654 cm^{-1}) absorption peaks.[33,34] After 5 min of the addition of NH_3, the peaks of the nitrate-like adsorbed species, adsorbed state NO_2, intermediate products $-NO_2$ and $-NO_3$ disappeared, along with the peaks of adsorbed NH_4^+ (1370, 1425, 1494 cm^{-1}), adsorbed NH_3 (1080, 1257 cm^{-1}) and $-NH_2$ (1309, 1530, 1560 cm^{-1}),[29,30] where the absorption peak of $-NH_2$ increased in intensity with time. The peak of adsorbed NH_3 was less variable, and the peak of adsorbed NH_4^+ disappeared quickly. Absorption peaks for NH_4^+ (1385, 1419, 1456, 1467, 1495 cm^{-1}) and $-NH_2$ (1625 cm^{-1}) adsorbed at the Brønsted acid site appeared after 20 min of the addition of NH_3.[29,30] When NH_3 was present, the $-NO_2$ and $-NO_3$ groups as well as the adsorbed NO_2 disappeared from the catalyst surface and NH_4^+ and $-NH_2$ groups were generated at subsequent time periods of the reaction, indicating that intermediate products NH_4NO_3, NH_4NO_2 and NH_2NO_2 were generated on the RET catalyst surface to remove NO adsorption products, suggesting that both the E–R mechanism and the L–H mechanism, which acted together to remove NO_x through both pathways.

4 Denitrification mechanism of SO_2/H_2O enhanced rare earth tailings catalyst

Combining the results of *in situ* DRIFTs analysis and SO_2 characterization,[22,23,38,39] We can surmise the following reaction mechanism (Fig. 10) as well as reaction equations (eqn (2)–(16)) can be derived for the effect of SO_2/H_2O on the RET catalysts. As shown in Fig. 10, combined with the analysis of the H_2-TPR results, it is found that the conversion between $Fe^{3+} \leftrightarrow Fe^{2+}$ and $Ce^{4+} \leftrightarrow Ce^{3+}$ on the RET catalyst surface provides the active sites for SCR catalytic denitrification, and the conversion between Ce^{3+} and Ce^{4+} mainly acts as oxygen storage and release (eqn (2)–(5)). When SO_2/H_2O is added, SO_2 is adsorbed by the hydroxyl groups formed by H_2O and reacts with O_2 to form SO_3^{2-} groups, while combining with SO_4^{2-} groups to form $S_2O_7^{2-}$ (eqn (7)–(9)). When NH_3 and NO are present, they are converted to NH_4^+ and NO_2^- respectively, which are then reduced to N_2 and H_2O (eqn (10)–(15)). The adsorption of H_2O by the catalyst surface increases the –OH sites on the catalyst surface, leading to easier adsorption and conversion of SO_2 to form SO_3^{2-}, while the $S_2O_7^{2-}$ group is converted to NH_3SO_3 and the unstable SO_4^{2-} group by the reduction of NH_3 (eqn (16)), allowing the catalyst reactive sites on the surface are restored, inhibiting the continued sulphation of the catalyst surface. NH_3 also adsorbs to the Brønsted and Lewis acidic sites on the RET catalyst surface as $-NH_2$ and NH_4^+, and perform NH_3-SCR reaction.

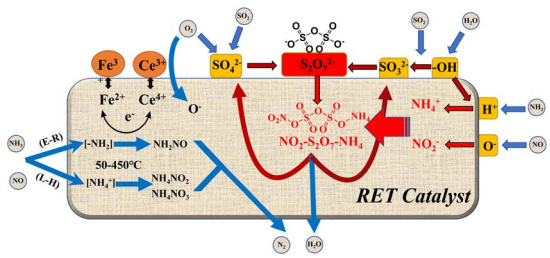

Fig. 10 Mechanism of SO_2/H_2O influence on the surface of rare earth tailings (RET) catalysts (△ represents the active metal sites on the RET catalyst surface; blue arrows represent the gas absorption and release process; black arrows represent the internal electron transfer process of the catalyst; red arrows represent the reaction cycle process of the $S_2O_7^{2-}$ group).

$$Fe^{3+} \leftrightarrow Fe^{2+} + \triangle \quad (2)$$

$$O_{2(g)} + 2\triangle \rightarrow 2O - \triangle \quad (3)$$

$$Ce^{3+} + O_{2(g)} \leftrightarrow Ce^{4+} + 2O^- \quad (4)$$

$$O^- + \triangle \rightarrow O - \triangle \quad (5)$$

$$H_2O_{(g)} + \triangle \rightarrow \triangle - OH + H^+ \quad (6)$$

$$\triangle - OH + SO_{2(g)} \rightarrow \triangle - SO_3^{2-} + H_2O \quad (7)$$

$$2SO_{2(g)} + 3/2O_{2(g)} + H_2O \rightarrow 2SO_4^{2-} + 2H^+ \quad (8)$$

$$SO_4^{2-} + \triangle - SO_3^{2-} \rightarrow \triangle - S_2O_7^{2-} \quad (9)$$

$$\triangle - S_2O_7^{2-} + H^+ \rightarrow \triangle - S_2O_7^{2-}H^+ \quad (10)$$

$$\triangle - S_2O_7^{2-}H^+ + NH_{3(g)} \rightarrow \triangle - S_2O_7^{2-}NH_4^+ \quad (11)$$

$$\triangle - S_2O_7^{2-}NH_4^+ + NO_{(g)} + 1/2O_{2(g)} \rightarrow \triangle - NO_2^- S_2O_7^{2-}NH_4^+ \quad (12)$$

$$\triangle - NO_2^- S_2O_7^{2-}NH_4^+ \rightarrow \triangle - S_2O_7^{2-} + N_{2(g)} + 2H_2O \quad (13)$$

$$\triangle - S_2O_7^{2-} + NH_{3(g)} \rightarrow \triangle - H_2NS_2O_7^{2-}H^+ \quad (14)$$

$$\triangle - H_2NS_2O_7^{2-}H^+ + NO_{(g)} \rightarrow \triangle S_2O_7^{2-}H^+ + N_{2(g)} + H_2O \quad (15)$$

$$\triangle - S_2O_7^{2-}H^+ + NH_{3(g)} + H^+ \rightarrow NH_3SO_3 + SO_4^{2-} + \triangle \quad (16)$$

where △ represents the surface oxygen vacancy in the active metal center. The symbol (g) represents NO, NH_3, SO_2, NO_2, N_2, and O_2 in the gaseous state. The symbol (a) represents the adsorbed state of NH_3, NH_4^+ and SO_3 on the catalyst surface.

5 Catalyst performance

5.1 Effect of H_2O and SO_2 on catalytic NO_X reduction

The effect of SO_2/H_2O on the catalytic denitrification activity of the RET catalyst was studied in the temperature range of 50–

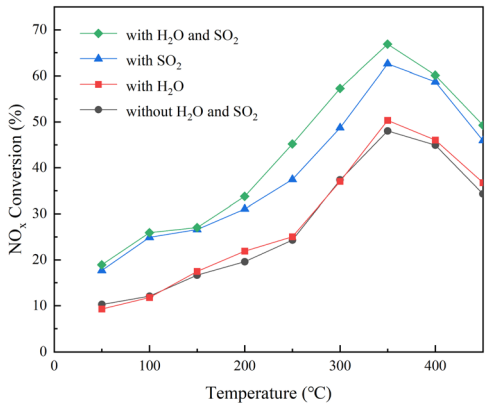

Fig. 11 RET catalyst NO_X removal rate.

450 °C with φNO, φNH_3 and φSO_2 of 500 × 10^{-6}, φO_2 of 6 × 10^{-2} and φH_2O of 6 × 10^{-2}. After the SCR reactor outlet φNO was stabilized for 10 min, the NH_3 was started to be introduced and the denitrification rate for each temperature section was calculated as the average of the NO_X outlet concentration values within 180 min of stabilization were calculated and the results, as shown in Fig. 11.

Fig. 11 shows that the NO_X conversion of the RET catalyst in the absence of SO_2/H_2O and SO_2 is much lower than that in the presence of SO_2 and H_2O, and H_2O has almost no effect on the NO_X conversion of the RET catalyst. At relatively low temperatures (50 to 200 °C), the enhancement of catalytic activity in the presence of SO_2 and H_2O was similar, about 10 ± 1%. However, when the reaction temperature is in the medium to high temperature range (250–450 °C), the activity enhancement under SO_2/H_2O can reach 16 ± 1%, and the activity enhancement of the RET catalyst in SO_2 only condition is only 10 ± 1%. Furthermore, at 350 °C, SO_2/H_2O in the gas supply leads to a significant increase in SCR activity of about 18 ± 1%, with a NO_X conversion of 66 ± 1% for the RET catalyst. This enhancement is due to SO_2 gas phase acidification of the active metal oxides under SO_2.[37] It suggests that the appropriate conditions of SO_2/H_2O presence are favorable to improve the catalytic activity of the RET catalysts.

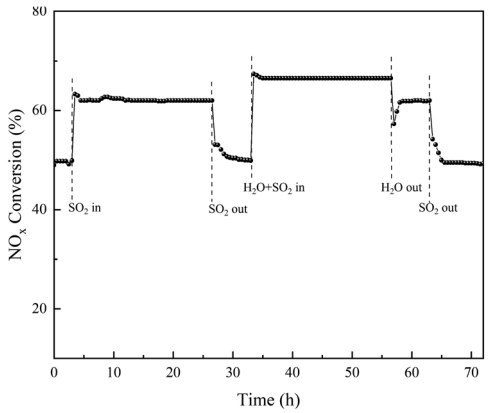

Fig. 12 Stability of RET catalyst NO_X removal rates under the influence of SO_2/H_2O.

With the same steps, the stability of the effect of SO_2/H_2O on the NO_X conversion in the temperature range of 350 °C of the RET catalyst over time is shown in Fig. 12 (the data points in the figure are the average values of NO_X conversion over 30 min).

Fig. 12 showed stable catalytic activity at 350 °C during the 72 h test. When SO_2 was added to the gas stream, the NO_X conversion increased from a stable 49 ± 1% in the first 3 h to obtain a stable NO_X conversion of 62 ± 1% in 24 h, indicating that SO_2 has a significant effect on the catalyst activity. The addition of SO_2/H_2O increases the catalytic activity from 49 ± 1% to 66 ± 1%. However, when H_2O is removed from the gas, the activity can be restored, implying that the enhancement effect of H_2O in promoting SO_2 influence on the activity is reversible. The NO_X conversion of the RET catalyst can be recovered when there is no SO_2 or H_2O in the reaction gas mixture, which proves that the RET catalyst has a good effect on SO_2/H_2O, and the SCR activity of the RET catalyst can be obtained at 350 °C with a 17 ± 1% enhancement under the conditions of both SO_2 and H_2O.

6 Conclusion

In summary, this paper prepared rare earth tailings (RET) catalysts from Bayan Ebo rare earth tailings by ball milling and microwave roasting, and analyzed the SO_2/H_2O tolerance mechanism of the RET catalysts by activity testing, characterization and *in situ* DRIFTs experiments. And revealed the mechanism of SO_2/H_2O to enhance the denitrification performance of catalysts by promoting the cyclic reaction of $S_2O_7^{2-}$ groups on the RET catalysts surface. Although RET catalysts are less active, they can be used as a catalyst active carrier through their excellent SO_2 tolerance properties.

(1) The effect of SO_2/H_2O on the RET catalyst was facilitated, and the NO_X conversion of the RET catalyst increased from 48% to 66 ± 1% at 350 °C under SO_2/H_2O, which was higher than that of SO_2 or H_2O alone.

(2) Rare earth tailings catalyst NH_3-SCR denitrification followed the combined L–H and E–R mechanism. The Fe^{n+}–Ce^{n+} coactivation of the RET catalyst provides Brønsted and Lewis acid sites.

(3) The effect of SO_2 on the RET catalyst is mainly the formation of SO_4^{2-} and SO_3^{2-} species, while H_2O promotes the formation of hydroxyl groups and facilitates SO_2 adsorption to form SO_3^{2-}, which promotes the reaction of SO_3^{2-} with SO_4^{2-} to form $S_2O_7^{2-}$ groups, which provide acid sites for the RET catalyst and improve the adsorption of NH_3. At the same time, the $S_2O_7^{2-}$ group decomposes into SO_3^{2-} and unstable SO_4^{2-} groups, thus continuing the cyclic reaction to form $S_2O_7^{2--}$ groups, thereby increasing the denitrification activity of the RET catalyst activity and inhibit the continued sulphation of the catalyst surface.

Conflicts of interest

There are no conflicts to declare.

Acknowledgements

The research was financially supported by the Natural Science Foundation of Inner Mongolia (Grant No. 2019ZD13).

References

1 K. Skalska, J. S. Miller and S. Ledakowicz, Trends in NOx abatement: A review, *Sci. Total Environ.*, 2010, **408**(19), 3976–3989.

2 G. L. Manney, L. Froidevaux, J. W. Waters, R. W. Zurek, W. G. Read, L. S. Elson, J. B. Kumer, J. L. Mergenthaler, A. E. Roche, A. O'Neill, R. S. Harwood, I. Mackenzie and R. Swinbank, Chemical depletion of ozone in the Arctic lower stratosphere during winter 1992-93, *Nature*, 1994, **370**(6489), 429–434.

3 D. Maric and J. P. Burrows, Formation of N_2O in the photolysis/photoexcitation of NO, NO_2 and air, *J. Photochem. Photobiol., A*, 1992, **66**(3), 291–312.

4 H. Bosch and F. Janssen, Catalytic reduction of nitrogen oxides-A review on the fundamental and technology, *Catal. Today*, 1988, **2**(4), 369–532.

5 G. Busca, L. Lietti, G. Ramis and F. Berti, Chemical and mechanistic aspects of the selective catalytic reduction of NOx by ammonia over oxide catalysts: A review, *Appl. Catal., B*, 1998, **18**(1–2), 1–36.

6 F. Kapteijn, L. Singoredjo and A. Andreini, Activity and selectivity of pure manganese oxides in the selective catalytic reduction of nitric oxide with ammonia, *Appl. Catal., B*, 1994, **3**(1), 173–189.

7 T. S. Park, S. K. Jeong, S. H. Hong and S. C. Hong, Selective catalytic reduction of nitrogen oxides with NH_3 over natural manganese ore at low temperature, *Ind. Eng. Chem. Res.*, 2001, **40**(21), 4491–4495.

8 L. Singoredjo, R. Korver and F. Kapteijin andJ.Moulijn, Alumina supported manganese oxides for the low-temperature selective catalytic reduction of nitric oxide with ammonia, *Appl. Catal., B*, 1992, **1**(4), 297–316.

9 C. Liu, S. Yang, L. Ma, Y. Peng, A. Hamidreza, H. Chang and J. Li, Comparison on the Performance of alpha-Fe_2O_3 and gamma-Fe_2O_3 for Selective Catalytic Reduction of Nitrogen Oxides with Ammonia, *Catal. Lett.*, 2013, **143**(7), 697–704.

10 A. Kato, S. Matsuda, T. Kamo, F. Nakajima, H. Kuroda and T. Narita, Reaction between NO_X and NH_3 on iron oxide-titanium oxide catalyst, *J. Phys. Chem.*, 1981, **85**(26), 276–287.

11 F. Liu, H. He and C. Zhang, Novel iron titanate catalyst for the selective catalytic reduction of NO with NH_3 in the medium temperature range, *Chem. Commun.*, 2008, **164**(17), 2043–2045.

12 F. Liu, H. He, C. Zhang, Z. Feng, L. Zheng, Y. Xie and T. Hu, Selective catalytic reduction of NO with NH_3 over iron titanate catalyst: Catalytic performance and characterization, *Appl. Catal., B*, 2010, **96**(3), 408–420.

13 F. Liu, K. Asakura, H. He, Y. Liu, W. Shan, X. Shi and C. Zhang, Influence of calcination temperature on iron titanate catalyst for the selective catalytic reduction of NO_X with NH_3, *Catal. Today*, 2011, **164**(1), 520–527.

14 L. Hou, S. Fu, X. Yan, C. Qiao and W. Wu, Effects of sulfate on denitration performance of rare earth tailings for selective catalytic reduction of NO with NH_3, *Mol. Cryst. Liq. Cryst.*, 2023, **755**(1), 91–106.

15 P. Zhang, Study on the process mineralogy of large-sized Bayan Obo Fe-REE-Nb deposit, *J. Chin. Rare Earth Soc.*, 1991, **9**(4), 350–353.

16 J. Wang, C. Zhu, B. Li, Z. Gong, Z. Meng, G. Xu and W. Wu, Prepare a catalyst consist of rare earth minerals to denitrate via NH_3-SCR, *Green Process. Synth.*, 2019, **9**(1), 191–202.

17 X. Bai, J. Lin, Z. Chen, L. Hou and W. Wu, A Study on the Effect of Different Ball Milling Methods on the NH_3-SCR Activity of Aluminum-Laden Bayan Obo Tailings, *Catalysts*, 2021, **11**(5), 568.

18 G. Qi and R. Yang, Low-temperature selective catalytic reduction of NO with NH_3 over iron and manganese oxides supported on titania, *Appl. Catal., B*, 2003, **44**(3), 217–225.

19 Z. Chen, F. Wang, H. Li, Q. Yang, L. Wang and X. Li, Low-Temperature Selective Catalytic Reduction of NO_X with NH_3 over Fe-Mn Mixed-Oxide Catalysts Containing Fe_3Mn_{30}s Phase, *Ind. Eng. Chem. Res.*, 2012, **51**(1), 202–212.

20 B. Shen, T. Liu, N. Zhao, X. Yang and L. Deng, Iron-doped Mn-Ce/TiO_2 catalyst for low temperature selective catalytic reduction of NO with NH_3, *J. Environ. Sci.*, 2010, **22**(9), 1447–1454.

21 F. Wang, B. Shen, S. Zhu and Z. Wang, Promotion of Fe and Co doped Mn-Ce/TiO_2 catalysts for low temperature NH_3-SCR with SO_2 tolerance, *Fuel*, 2019, **249**, 54–60.

22 E. Hartley and M. J. Matteson, Sulfur dioxide reactions with ammonia in humid air, *Ind. Eng. Chem. Fundam.*, 1975, **14**(1), 67–72.

23 Z. Gao, W. Yang, X. Ding, G. Lv and W. Yang, Support effects in single atom iron catalysts on adsorption characteristics of toxic gases (NO_2, NH_3, SO_3 and H_2S), *Appl. Surf. Sci.*, 2018, **436**, 585–595.

24 L. Liu and Z. Yuan, Ordered Mesoporous Carbon Materials Synthesized by Organic-Organic Self-Assembly, *Prog. Chem.*, 2014, **26**(05), 756–771.

25 X. Zhu, Y. Wang, Y. Huang and Y. Cai, Selective catalytic reduction of NO with NH_3 over Ce-W-Ti oxide catalysts prepared by solvent combustion method, *Appl. Sci.*, 2018, **8**(12), 2430.

26 F. Liu and H. He, Structure-Activity Relationship of Iron Titanate Catalysts in the Selective Catalytic Reduction of NO_X with NH_3, *J. Phys. Chem. C*, 2010, **114**(40), 16929–16936.

27 X. Huang, P. Wang, J. Tao and Z. Xi, CeO_2-modified Mn-Fe-O composites and their catalytic performance for NH_3-SCR denitrification, *J. Inorg. Mater.*, 2020, **35**(05), 573–580.

28 Q. Fu, J. Wen, L. Li, Y. Xiao and K. Gao, The Study of REE Occurrence State in Bayan Obo Tailings, *Chin. Rare Earths*, 2017, **38**(05), 103–110.

29 J. Sun, Y. Lu, L. Zhang, C. Ge, C. Tang, H. Wan and L. Dong, Comparative Study of Different Doped Metal Cations on the Reduction, Acidity, and Activity of $Fe_9M_1O_X$ (M= Ti^{4+}, $Ce^{4+/3+}$, Al^{3+}) Catalysts for NH_3-SCR Reaction, *Ind. Eng. Chem. Res.*, 2017, **56**(42), 12101–12110.

30 G. Ramis and M. A. Larrubia, An FT-IR study of the adsorption and oxidation of N-containing compounds over Fe_2O_3/Al_2O_3 SCR catalysts, *J. Mol. Catal. A: Chem.*, 2004, **215**(1–2), 161–167.

31 A. A. Ioffe, V. P. Bulatov, V. A. Lozovsky, M. Y. Goldenberg, O. M. Sarkisov and S. Ya, Umansky. On the reaction of the NH_2 radical with SO_2 at 298–363 K, *Chem. Phys. Lett.*, 1989, **156**(5), 425–432.

32 D. Ye, R. Qu, C. Zheng, K. Cen and X. Gao, Mechanistic investigation of enhanced reactivity of NH_4HSO_4 and NO on Nb- and Sb- doped V-W/Ti SCR catalysts, *Appl. Catal., A*, 2018, **549**, 310–319.

33 F. Liu and H. He, Selective catalytic reduction of NO with NH_3 over manganese substituted iron titanate catalyst: Reaction mechanism and H_2O/SO_2 inhibition mechanism study, *Catal. Today*, 2010, **153**(3–4), 70–76.

34 L. Chen, X. Yao, J. Cao, F. Yang, C. Tang and L. Dong, Effect of Ti^{4+} and Sn^{4+} co-incorporation on the catalytic performance of CeO_2-MnO_X catalyst for low temperature NH_3-SCR, *Appl. Surf. Sci.*, 2019, **476**, 283–292.

35 F. Gao, X. Tang, H. Yi, S. Zhao, J. Wang and T. Gu, Improvement of activity, selectivity and $H_2O\&SO_2$-tolerance of micro-mesoporous $CrMn_2O_4$ spinel catalyst for low-temperature NH_3-SCR of NO_X, *Appl. Surf. Sci.*, 2019, **466**, 411–424.

36 S. Pan, H. Luo, L. Li, Z. Wei and B. Huang, H_2O and SO_2 deactivation mechanism of MnO_X/MWCNTs for low-temperature SCR of NO_X with NH_3, *J. Mol. Catal. A: Chem.*, 2013, **377**, 154–161.

37 T. Gu, L. Yue, H. Wang and Z. Wu, The enhanced performance of ceria with surface sulfation for selective catalytic reduction of NO by NH_3, *Catal. Commun.*, 2010, **12**(4), 310–313.

38 W. S. A. El-Yazeed, M. Eladl, A. I. Ahmed and A. A. Ibrahim, Sulfamic: acid incorporated tin oxide: Acidity and activity relationship, *J. Alloys Compd.*, 2021, **858**, 158–192.

39 E. Hayon, A. Treinin and J. Wilf, Electronic spectra, photochemistry, and autoxidation mechanism of the sulfite bisulfite pyrosulfite systems. SO2-, SO3-, SO4-, and SO5-radicals, *J. Am. Chem. Soc.*, 1972, **94**(1), 47–57.